ELSEVIER

Coordination Chemistry Reviews
183 (1999) 3–18

COORDINATION CHEMISTRY REVIEWS

Binding and two-dimensional crystallization of streptavidin at the air/water interface via engineered Cu-IDA chelator lipids

Kevin M. Maloney [1,a], William R. Schief Jr. [b], Daniel W. Pack [2,a], Wolfgang Frey [3,b], Frances H. Arnold [a], Viola Vogel [b,*]

[a] *Department of Chemistry and Chemical Engineering, California Institute of Technology, Mailcode 210-41, Pasadena, CA 91125, USA*
[b] *Department of Bioengineering, University of Washington, Box 352125, Seattle, WA 98195, USA*

Received 6 January 1998

Contents

* Corresponding author. Fax: +1-206-685-4434; e-mail: vogel@bioeng.washington.edu
[1] Present address: Amgen Inc., 1840 DeHavilland Drive, Thousand Oaks, CA 91320, USA.
[2] Present address: Department of Chemical Engineering, University of Illinois, Urbana, IL 61801, USA.
[3] Present address: Department of Biomedical Engineering, Duke University, Durham, NC 27708-0281, USA.

PII S0010-8545(98)00174-X

Abstract

Metal-chelating iminodiacetate (IDA) lipid monolayers at the air/water interface have been engineered to promote the 2D crystallization of proteins which display solvent-accessible histidines. The physical properties of IDA lipid monolayers have been specifically tailored to allow the binding and 2D assembly of added proteins. Fluorescently labeled IDA lipid monolayers allow us to monitor the formation of the protein crystals optically. Here we review our efforts in the interfacial crystallization of streptavidin as monitored using fluorescence, Brewster angle and transmission electron microscopy and discuss future challenges in this area.

Keywords: Air/water interface; Brewster angle microscopy; Cu(II); Fluorescence microscopy; Iminodiacetate; Metal-chelating lipids; Monolayers

1. Introduction

Synthetic self-assembled lipid architectures are simple and robust scaffolds for targeting and organizing water-soluble biomolecules in two and three dimensions (2D and 3D) [1]. Typical lipid architectures include bilayers, tubules, micelles, hexagonal phases and lipid monolayers at the air/water interface. The variety of architectures adopted by lipids makes them useful in both basic and applied membrane chemistry. Lipid/aqueous interfaces have been used as scaffolds for crystallization and structural characterization of biological molecules in 2D via electron microscopy [2,3] and have inspired research in biomimetic materials fabrication and processing [4–6].

Two-dimensional lipid monolayers at the air/liquid interface [7] are particularly useful lipid assemblies for studying interfacial protein crystallization. Protein binding to interfacially tethered receptors followed by spontaneous protein self-organization can be controlled by tuning physical properties at the lipid/aqueous interface [1]. Useful parameters include the lateral density of lipid receptor sites, surface phase, surface charge, and lipid monolayer surface pressure [7]. An especially important monolayer property which affects protein binding and crystallization is monolayer fluidity [2,8]. It is well recognized that solid-like lipid monolayers are often ineffective at promoting protein self-assembly with long-range order. The main driving force for 2D protein crystallization is generally believed to be the large apparent surface concentration of bound protein which can be several orders of magnitude larger than that of the bulk phase [2,8,9].

Prior work in lipid monolayer-promoted protein crystallization can generally be classified by the type of recognition element used to target a protein to the lipid surface. Specific protein active site receptors [10–14], non-specific electrostatic binding interactions between a protein's surface and the lipid interface [15–17], and general protein receptors capable of binding specific surface accessible amino acid motifs unrelated to the protein active site [18–21] have been used. We and others have focused our efforts on this latter strategy and have employed metal-chelating

lipids which recognize and bind proteins via solvent accessible histidine residues (Fig. 1) [18–20,22,23].

The tridentate iminodiacetate (IDA) functionality in the hydrophilic headgroup strongly chelates divalent metal ions {for Cu(II), $K_a \approx 10^{10}\,M^{-1}$ [24]}. IDA is tethered to hydrocarbon tails via a triethyleneoxide spacer arm to ensure the IDA moiety is accessible for exogenous ligand binding. The metal-bound lipid can coordinate additional ligands such as the histidyl side chain at neutral pH or amines at alkaline pH (e.g. deprotonated lysine) [25]. The binding constant for single histidyl coordination to the Cu-IDA complex is $10^{3.5}\,M^{-1}$ [25], which is reversible by lowering or adding a competitive metal chelator such as ethylenediaminetetraacetatic acid (EDTA). At neutral pH, histidine is generally the only amino acid which binds significantly to Cu-IDA. Although single histidine binding is of moderate affinity, binding interactions can be enhanced significantly by the simultaneous binding of multiple histidines to the Cu-IDA surface [25,26].

Since most proteins contain solvent accessible histidine residues, this targeting mechanism is applicable to a variety of proteins. In the case that a protein lacks accessible histidines, it could be genetically engineered to present a variety of metal

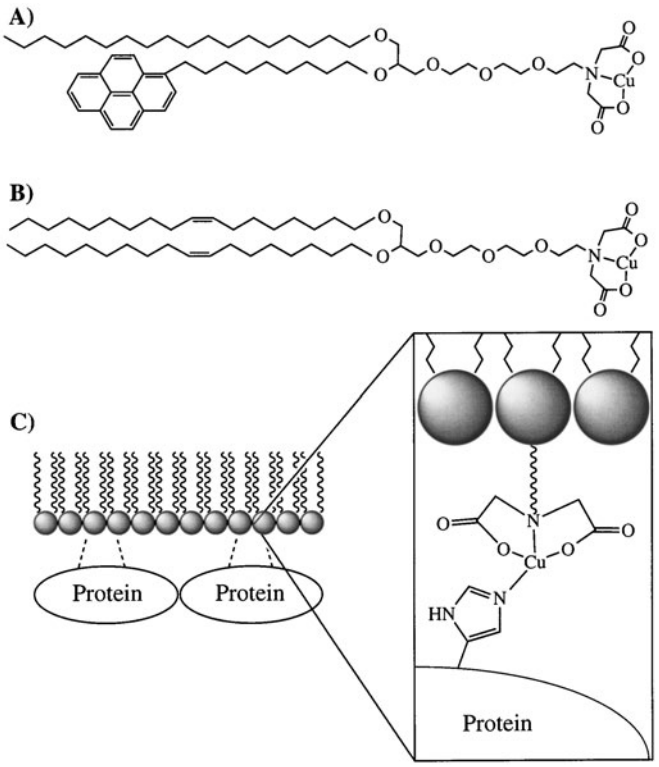

Fig. 1. Protein targeting to metal-chelating lipids via histidine coordination to Cu-IDA. Chemical structures of (A) Cu-PSIDA and (B) Cu-DOIDA metal-chelating IDA lipids.

binding motifs [27,28]. This latter method is frequently employed in the purification of recombinant proteins using histidine tags and immobilized metal affinity chromatography (IMAC) [27]. Although the tetradentate nitrilotriacetate (NTA) ligand is often used with Ni(II) as an IMAC support, Ni-NTA binds single histidines poorly [29] and is only effective with polyhistidine-tagged proteins. Because Cu-IDA can bind both native and recombinant proteins which contain surface accessible histidines, it is a more versatile protein receptor.

Here we review our efforts in targeting and crystallizing the water-soluble tetramer streptavidin to metal-chelating Cu-IDA lipid monolayers at the air/water interface and compare our results to streptavidin crystallization using biotinylated lipid monolayers. 2D streptavidin crystallization was investigated using two Cu-IDA lipids which differ chemically in their hydrocarbon tails. Long-range 2D streptavidin crystal formation was observed in situ with Brewster angle microscopy (BAM) and fluorescence microscopy. Transmission electron microscopy (TEM) was also employed for molecular-level crystal lattice parameter determination.

2. Lipid monolayer-promoted streptavidin crystallization

Biotinylated lipid monolayers are well known to bind strongly to streptavidin (biotin–streptavidin solution $K_a \approx 10^{15}\ M^{-1}$ [51]) and promote 2D crystallization [1,11]. Inspection of streptavidin three-dimensional tetrameric crystal structure [30–33] reveals a solvent accessible histidine residue (His 87) in close proximity to each biotin binding pocket as well as a less accessible residue (His 127) located in a cleft on the side of the protein barrel [34]. Owing to the symmetry of streptavidin, we expected that at least two histidines would be accessible for interaction with the lipid monolayer. Since streptavidin already exhibits favorable intermolecular interactions which allow 2D crystallization at biotinylated lipid interfaces, we set out to crystallize the protein using Cu-DOIDA [Fig. 1(B)] monolayers. We specifically wanted to determine whether the Cu(II)-IDA–histidine binding interaction, which is ca. 12 orders of magnitude weaker than the biotin–streptavidin interaction, could still promote interfacial binding and crystallization. We were also interested in determining if changes in streptavidin crystal morphology and differences in crystallization properties would result from assembling the protein via the Cu(II)-IDA–histidine interaction.

2.1. Crystal detection via Brewster and fluorescence microscopy

Optical microscopy of lipid monolayers at air/water interfaces is a convenient method for observing in situ the interfacial assembly of exogenous proteins. Formation of large 2D protein arrays beneath lipid monolayers can be monitored readily using BAM [34,35] and fluorescence microscopy [36]. Fluorescence microscopy relies on the addition of a photolabel to either the protein or the lipid monolayer for contrast, but the contrast mechanism in BAM requires no label. Contrast in BAM is due to the changes in interfacial optical thickness which occur

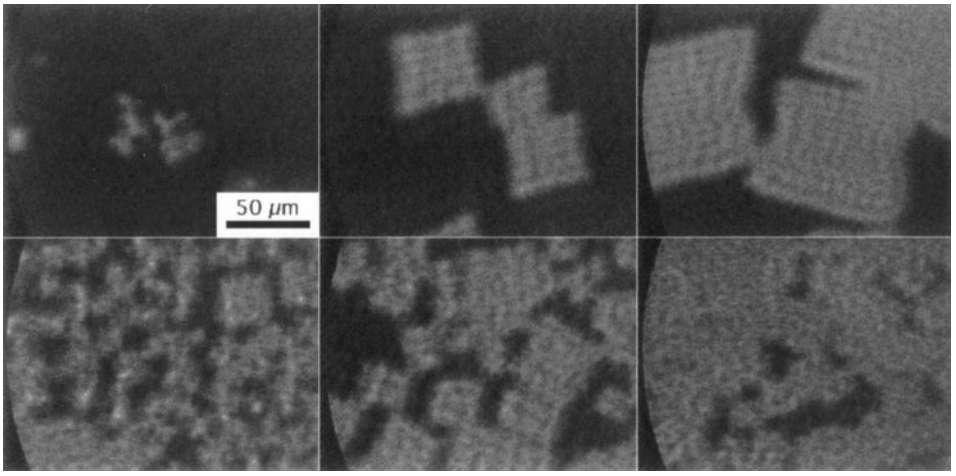

Fig. 2. Brewster angle microscopy of streptavidin crystals beneath 100% Cu-DOIDA monolayers. Monolayer subphase was 250 mM NaCl, 20 mM MOPS, pH 7.8, room temperature. Protein was injected to a bulk concentration of 133 nM beneath the lipid monolayer which had previously been compressed to a surface pressure of 3 mN m^{-1}. The crystals appear bright on a darker background owing to the higher protein surface density inside the crystal. This figure illustrates the nucleation and growth of the crystals in both sparsely nucleated regions (top row) and densely nucleated regions (bottom row) under the same lipid monolayer. From left to right, the images in both rows were taken at times after protein injection of ca. 15, 65, and 190 min.

upon protein binding and crystallization. For the case of streptavidin, variation in the BAM image greyscale can be analyzed quantitatively in terms of the protein surface density (see Section 2.2) [34,35,37,38].

When streptavidin is injected beneath a Cu-DOIDA monolayer resting at 3 mN m^{-1}, the protein binds rapidly and forms 2D crystals. Visualized by BAM, Fig. 2 depicts the formation and growth of streptavidin arrays beneath pure Cu-DOIDA monolayers. Shortly after protein injection beneath the monolayer, small crystals appear (Fig. 2, left) and grow clearly rectangular with time (Fig. 2, center) until they cover essentially the entire lipid surface (Fig. 2, right). Notably, the rectangular morphology of streptavidin crystals obtained with Cu-DOIDA lipids differs from morphologies under biotinylated lipid monolayers, which yield H- or X-shaped streptavidin crystals [39,40]. This difference in shape is especially striking since the lattice parameters of the two crystals are identical at 15 Å resolution (see Section 3 for a discussion of TEM data and the possible origin of the difference in crystal shape).

2.2. Critical interfacial streptavidin density

To gain quantitative information on the thermodynamics of the non-crystalline to crystalline phase transition, we analyzed the BAM image greyscale to obtain the relative protein surface density of both phases separately as a function of time.

Previously, we showed the BAM greyscale versus time [35], and now with recent information from electron microscopy on the crystal unit cell (see Section 3) we are able to convert the greyscale into protein surface density relative to the crystal density. Fig. 3 shows a plot of the relative protein surface density and the protein layer refractive index of both phases versus time after protein injection. An explanation of the calculation of the relative protein surface density is provided in the caption to Fig. 3.

Following protein injection the non-crystalline protein density rises within 15 min to 20(+ 10/ − 5)% of the crystalline density and remains constant thereafter. When the relative density of the non-crystalline phase reaches the plateau, crystals appear with a much higher greyscale, hence a higher density, and the crystal greyscale then remains constant. The abrupt appearance of the crystal phase following a density increase in the non-crystal phase, and the subsequent constant density of both phases, indicate that this transition is of first order. The critical streptavidin density necessary for the formation of crystals is 20% of the crystal density. This is rather low in comparison with the critical protein density needed for crystal growth using biotinylated monolayers (75% [41]).

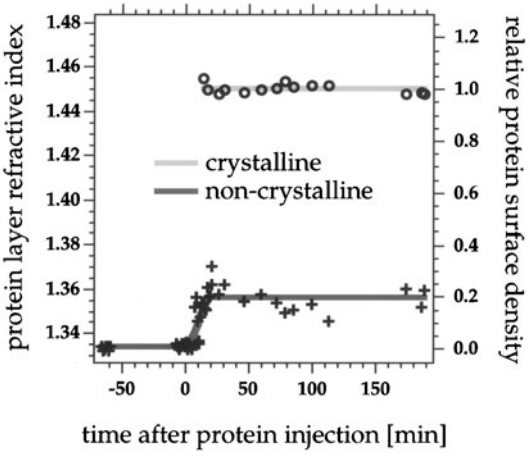

Fig. 3. Protein layer refractive index and corresponding relative protein surface density for both the non-crystalline and crystalline phases, plotted versus the time after protein injection. The BAM image greyscales are linearly related to the reflectivities of the interface. The reflectivity in turn can be converted to a relative protein surface density through the Fresnel equations and a Maxwell–Garnett model, as described in detail in Ref. [41]. The protein surface density is given relative to the density within the 2D crystals, which can be calculated from the unit cell determined by electron microscopy to be ~ 3600 Å^2 per protein (see Section 3). For the present analysis, we have assumed the refractive index and thickness of the Cu-DOIDA monolayer to be the same as those measured for a biotin-X-DPPE monolayer; values are given in Ref. [41]. The uncertainty in the relative surface density introduced by this assumption has been determined to be less than (+ 10/ − 5)% by comparing results of the greyscale conversion over a wide parameter space ($1.4 \leq$ refractive index ≤ 1.7; 10 Å $\leq$ thickness $\leq$ 25 Å).

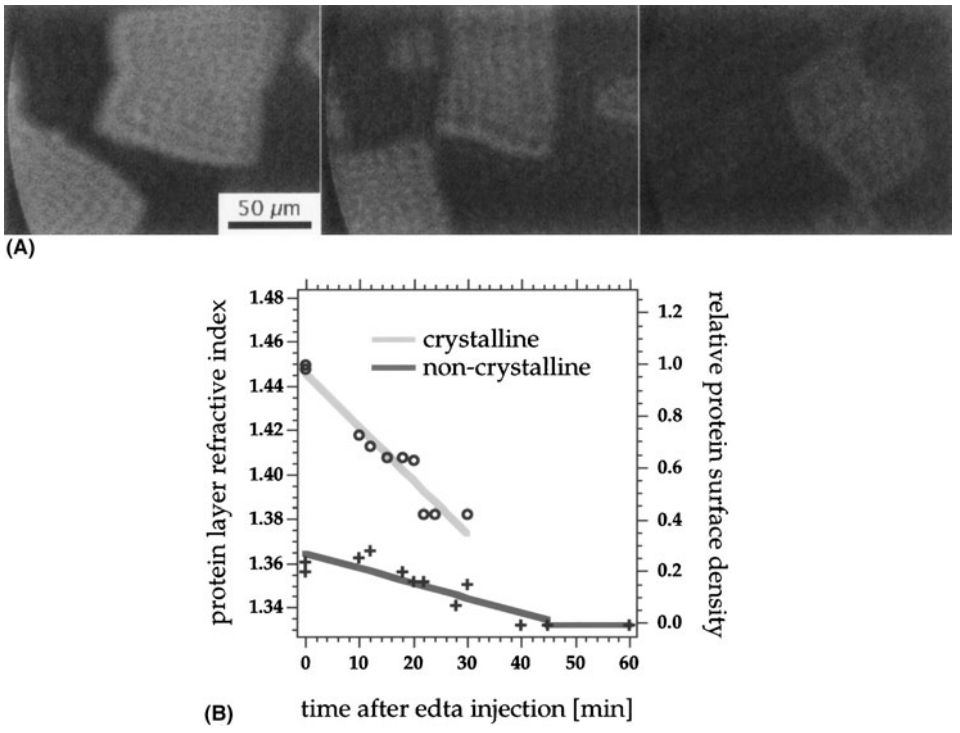

Fig. 4. (A) Sequence of BAM images depicting crystal dissolution following the injection of EDTA beneath streptavidin-covered Cu-DOIDA monolayers. EDTA was injected to a bulk concentration of 200 μM (ca. 1.5×10^3 excess over streptavidin). From left to right, the images show typical crystals prior to EDTA injection, 10 min after injection, and 14 min after injection. After 30 min the crystals were no longer visible. (B) BAM image greyscale and normalized protein surface density for both the non-crystalline and crystalline phases, plotted versus time after EDTA injection. This graph quantitatively demonstrates that the presence of EDTA causes the protein to desorb from the interface. As the crystals dissolve, their density falls toward the non-crystalline density. The crystals completely disappear 30 min after EDTA injection. Importantly, the non-crystalline surface density also decreases. 45 min after EDTA injection, the BAM greyscale has returned to the greyscale of the plain lipid layer, demonstrating that essentially all of the protein has desorbed from the interface. Protein density was calculated from the image greyscale as discussed in Fig. 3.

2.3. Binding mechanism: proof of principle

In order to prove that the surface binding of streptavidin to Cu-IDA lipid monolayers is indeed mediated by copper, two experiments were performed. First, streptavidin was injected underneath an IDA monolayer with Cu absent from both the monolayer and the subphase. In this case, streptavidin did not bind to the monolayer. Second, the metal scavenger EDTA was injected into the subphase after 2D streptavidin crystals had been grown beneath a Cu-IDA lipid monolayer. In this case, EDTA competed successfully with surface histidines for Cu(II), causing the crystals to fade away within a few minutes [Fig. 4(A)]. Streptavidin desorbed from

the interface and the grayscale dropped back to the value prior to protein injection [Fig. 4(B)].

Since streptavidin possesses two surface histidines (eight total in the tetramer), additional control experiments were conducted with recombinant forms of core streptavidin to assess the role H87 and H127 residues play in protein binding to Cu-DOIDA lipid monolayers. A site-directed mutant of streptavidin in which H127 had been replaced by cysteine (H127C) [34,42] was observed by BAM to bind and crystallize beneath Cu-DOIDA monolayers similar to the native protein, indicating that His 127 does not play a role in protein binding. A structural analysis of streptavidin also indicates that the length of the Cu-DOIDA ethyleneoxide headgroup spacer is not sufficient to bind His 127, which resides in a deep cleft. The H87 to alanine mutant, on the other hand, failed to crystallize underneath Cu-DOIDA monolayers. Even after a several hour incubation period with 250 nM H87A in the subphase, no binding to the Cu-DOIDA surface was observed, as confirmed by a BAM image greyscale analysis [35]. Results from mutant streptavidin control experiments clearly implicate H87 as the residue responsible for protein binding to Cu(II)-DOIDA monolayers, consistent with the EDTA and imidazole injection experiments discussed earlier in this section.

2.4. Importance of monolayer physical state on crystal formation and stability

Cu-DOIDA lipid tails contain oleyl hydrocarbons, a chemical feature intentionally designed into the lipid. It is well known that lipid monolayers exhibiting 2D solid or condensed phases are poor scaffolds for the binding and interfacial assembly of many proteins [8]. In the light of this general observation, lipids containing mono- or di-unsaturated hydrocarbon chains are frequently employed in 2D protein crystallization. Monolayer fluidity (i.e. large isothermal compressibility) facilitates interfacial reorganization of both lipid and bound protein, a process crucial for long-range protein assembly. Streptavidin crystallization experiments shown in Figs. 2 and 4 were intentionally conducted at low surface pressures ($3\ mN\ m^{-1}$) to ensure the Cu-DOIDA film would exhibit a liquid-like state. Surface pressure–area isothermal compression and fluorescence microscopy data support this physical picture [22,43]. When crystallization experiments are attempted at high surface pressures (near $20\ mN\ m^{-1}$), Cu-DOIDA films are less compressible than the corresponding monolayer at 3 mN/m and do not promote protein crystallization.

The robustness of streptavidin crystals formed beneath Cu-DOIDA monolayers is also sensitively linked to the monolayer physical state. Formation of crystals at low pressure, followed by a compression of the monolayer (surface area reduction of 45%), results in crystal disruption and protein desorption from the interface [35]. On the other hand, expansion of a crystal-bound Cu-DOIDA monolayer leads to crystal disassembly, although rapid recrystallization does occur [35]. Recrystallization is possible when the monolayer is expanded because the monolayer remains fluid.

2.5. Long-range microscopic order within individual streptavidin crystals

The growth of streptavidin crystals beneath Cu-DOIDA monolayers can also be observed with fluorescence microscopy. Small, rectangular rhodamine-labeled streptavidin crystals are initially apparent [Fig. 5(A)] and continue to grow until large crystals are formed and essentially cover the entire lipid surface [Fig. 5(C) and (D)]. The presence of a photolabel evidently does not interfere with the binding or crystallization of streptavidin since the growth process with labeled protein is very similar to that seen in BAM with unlabeled protein under similar conditions.

Polarized fluorescence from streptavidin crystals underneath both Cu-DOIDA and biotinylated lipid monolayers demonstrated the persistence of long-range order in those 2D crystals [40]. Fig. 5(C) and (D) were obtained from the same monolayer field of view and were visualized with two rhodamine excitation polarizations which differ by 90°. Crystals which appear bright in Fig. 5(C) invert their intensities when a polarizer is rotated through 90° [Fig. 5(D)], indicating that order persists throughout individual protein crystals [40]. The fact that entire crystals invert, rather than smaller patches within each crystal, indicates that these are single

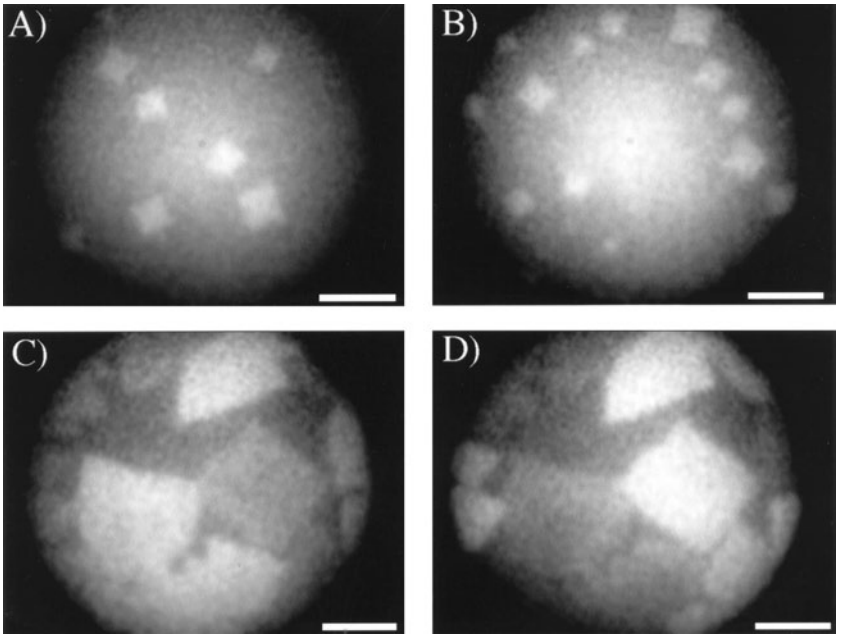

Fig. 5. Fluorescence microscopy of rhodamine–streptavidin crystals beneath 100% Cu-PSIDA monolayers. Monolayer subphase is 150 mM NaCl, 20 mM MOPS, pH 7.8, room temperature. Streptavidin was labeled with rhodamine following a routine procedure [44], yielding typical labeling ratios of 1.5 rhodamine/protein. Protein injected beneath monolayer at an initial surface pressure of 3 mN m^{-1}. Rhodamine–streptavidin fluorescence images in (A) show the onset of crystallization. Polarized rhodamine fluorescence images in (C) and (D) taken at the end of crystallization are of the same monolayer field of view. Incident excitation light in (D) is rotated 90° relative to (C). Scale bar is 100 μm.

crystals. A few protein arrays do not invert their fluorescence emission intensities while excitation polarization is rotated by 90° (the protein domains do not change their intensities at any angle between 0 and 90°). Assuming that streptavidin is uniquely labeled with rhodamine [40], these domains are apparently not well ordered over this large length scale.

The origin of the polarized fluorescence has not been determined. For polarized fluorescence, the fluorophores must attach to the proteins in such a way that their orientation is restricted to lie along a preferred axis within the crystal. That the fluorophores are largely immobilized is somewhat surprising, since they are expected to attach to single surface residues. Given that the fluorophores are immobilized, however, the 222 point group symmetry of the streptavidin tetramer [32] combined with the *C*222 symmetry of the crystal lattice (see Section 3) does provide a basis for a preferred fluorophore orientation within the crystal. For example, in certain cases in which the photolabel is immobilized preferentially to one residue with the fluorophore aligned along a symmetry axis in the protein, the protein's tetrameric symmetry will align that fluorophore with other fluorophores bound to the same residue on other monomers of the tetramer. Owing to the symmetry of the crystal lattice, such alignment would be propagated throughout the crystal.

It is important to note here that 2D streptavidin crystals do not exhibit optical anisotropy in BAM. BAM can resolve inherent optical anisotropy caused by collective tilting of hydrocarbon chains in lipid monolayers with the use of an analyzer in the reflected beam [45]. The resolution of our system allows clear visualization of such anisotropy in condensed lipid monolayer phases, but we have detected no inherent anisotropy in streptavidin crystals bound either to Cu-IDA monolayers or biotinylated monolayers. Given the symmetry of the 2D crystal lattice, the lack of inherent anisotropy indicates that the protein molecules themselves are optically isotropic at our level of detection.

3. Streptavidin crystal lattice parameters and their relation to crystal shape

BAM and fluorescence microscopy provide structural and dynamic information on the micrometer scale. For molecular level structural information, additional characterization techniques are required. Once protein crystals have formed beneath the lipid monolayer, they can be transferred to solid supports [46]. Streptavidin crystals obtained with Cu-DOIDA monolayers have been transferred to electron microscopy grids, negatively stained, and imaged via TEM [47].

Images obtained from specimens of Cu-DOIDA-bound streptavidin, which revealed large aggregates by BAM, showed clear crystalline packing by electron microscopy [47]. The lattice parameters were determined as $a = 85.2$ and $b = 85.7$ Å (Table 1). For comparison, those for the biotin-bound 2D streptavidin crystals in vitreous ice [3] were measured as $a = b = 82.3$ Å, and in negative stain as $a = b =$ 84 Å. An analysis of the symmetry present in the 2D crystals of streptavidin complexed to the Cu-DOIDA lipids revealed that the phase residuals for the 2-fold

Table 1
Lattice vectors and phase residuals for 2-fold symmetry along the principal lattice vectors for streptavidin 2-D crystals obtained using Cu-DOIDA lipids and DPPE-X-biotin lipids [3]

Crystal form	Lattice vectors (Å)		Phase residual (°)	
	a	*b*	*a*	*b*
SA/Cu-DOIDA[a]	85.2 (0.4)	85.7 (0.5)	5.9 (2.1)	12.4 (6.2)
SA/DPPE-X-biotin[b]	82.3	82.3	18.0	15.0
SA/DPPE-X-biotin[c]	84 ± 1	85 ± 1	5.3 [P2] 7.7 [C222]	

Numbers in parentheses denote the standard deviations over 58 measurements. For comparison the results for DPPE-X-biotin-bound streptavidin crystals [9] are shown.
[a] Ref. [47]. [b] Ref. [3]. [c] Ref. [9].

symmetry along the lattice vectors are very similar to those for the vitreous ice-embedded crystals of streptavidin bound to biotin lipid (Table 1). This suggests that the symmetry was the same, i.e. *C*222. The lower residuals for the stained crystals simply reflect the larger diffractive power caused by the stain. The relatively minor difference in both lattice spacings is considered to reflect differences in preparative conditions.

The somewhat surprising finding of the same symmetry and lattice constants in both the square-shaped crystals formed under Cu-DOIDA and the H-shaped crystals formed under biotinylated lipid monolayers has led to the postulation of a kinetic basis for the shape difference [47]. It is possible that a structural difference between the proteins in differently shaped crystals exists below the ~ 15 Å resolution of the recent TEM work, since biotin binding has been reported to cause structural changes in streptavidin [32] and coordination of surface histidines to Cu-IDA would not be expected to cause significant structural changes. However, the shape difference might also be explained by a model which takes into account some of the in-plane kinetics of protein attachment onto the crystal edge [47]. More experiments and higher resolution TEM work on DOIDA crystals are necessary to determine which model is correct.

4. Effect of Cu-IDA dilution on binding and crystallization

Coordination of streptavidin to Cu-IDA monolayers via two histidine residues is expected to be weak relative to streptavidin binding to two biotinylated lipids ($\sim 10^7$ versus $\sim 10^{30}\ M^{-1}$). We investigated the impact on streptavidin binding and crystallization of reducing the density of Cu-IDA groups in lipid monolayers at fixed surface pressures. Using binary lipid mixtures, we varied the mol% of Cu-IDA in the monolayer. In addition, we examined the impact of steric restriction of the Cu-IDA headgroup on crystallization by mixing Cu-IDA with non-binding lipids that exhibit varied steric packing properties. Experiments were performed with

mixtures of either Cu-DOIDA or Cu-PSIDA (see Section 5) and one of three diluent lipids: a PSIDA derivative lacking the IDA headgroup but containing identical hydrocarbon chains, backbone and ethyleneoxide spacer (PSOH), and the naturally occuring phosphatidylcholines SOPC and DOPC. Though the PC headgroup is large enough to sterically reduce the mobility of the upper part of the spacer on the Cu-IDA lipid, the PSOH lipid containing the ethyleneoxide spacer is expected to restrict the Cu-IDA motions even further. (In condensed monolayers of pure DPPC at 42 mN/m the headgroup extends 9 Å into the subphase [48]. With our monolayers at 3 mN/m, we expect the PC headgroup to extend less far into the subphase.) Fig. 6 illustrates the expected steric differences between Cu-PSIDA/SOPC mixtures and Cu-PSIDA/PSOH mixtures.

Despite the expected steric differences, dilution by either SOPC or PSOH showed the same results. By fluorescence microscopy and BAM, we were unable to observe crystallization of streptavidin with Cu-PSIDA monolayers mixed with either PSOH or SOPC when the Cu-PSIDA mole fraction was < 0.4. Indeed, BAM greyscale analysis of Cu-PSIDA/PSOH mixtures showed no evidence for protein binding with Cu-IDA mole fraction below 33%. Compared to the biotin–streptavidin system, the required surface mole fractions of Cu-IDA lipid for protein crystallization are at least ten times larger. Biotin lipid monolayer systems can promote binding and crystallization of streptavidin with a biotin lipid mole fraction as low as 2.3% [49]. The IDA and biotin mole fraction cut-off behaviors presumably reflect the low binding affinity of streptavidin for Cu-IDA versus biotin. Since the binding constant for streptavidin to biotin is 12 orders of magnitude stronger than for Cu-IDA, the kinetic off-rate with Cu-IDA systems is presumed to be much higher. Therefore, at low Cu-IDA surface concentrations, desorption of protein from the interface is more likely to lead to diffusion to the bulk aqueous phase rather than

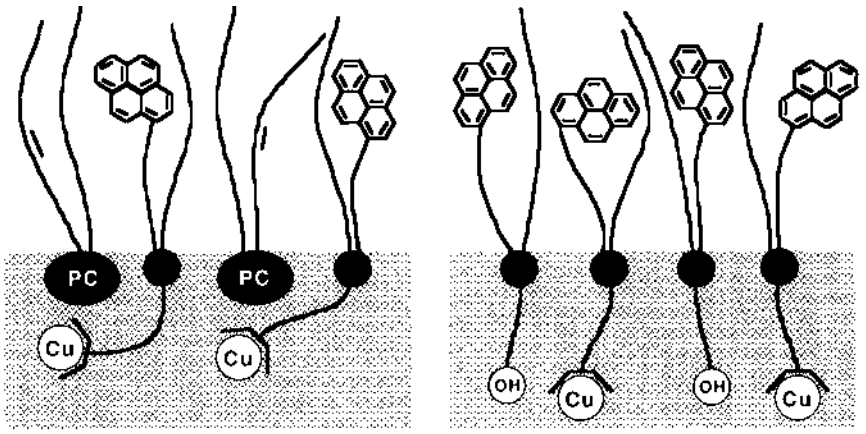

Fig. 6. Schematic of mixed lipid layers used to study the effect of binding site dilution on protein binding and crystallization. (A) Cu-PSIDA/SOPC monolayer. (B) Cu-PSIDA/PSOH monolayer. Despite the increased steric restriction expected in the case of dilution with PSOH, crystallization results were the same: both systems failed to promote streptavidin crystallization with < 40 mol% Cu-PSIDA.

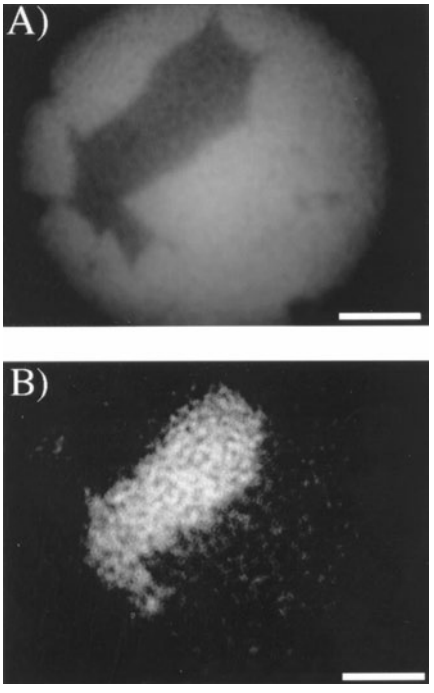

Fig. 7. Fluorescence micrographs from double label experiment with rhodamine–streptavidin crystals beneath 100% Cu-PSIDA monolayers. Subphase conditions are the same as in Fig. 5. Image (A) is the same monolayer field of view as image (B). Quenched regions of Cu-PSIDA excimer emission in (B) correspond to regions of bright rhodamine–streptavidin fluorescence in (A). Scale bar is 100 μm.

rebinding to the surface (not allowing further nucleation and crystal growth). The fact that the same mole fraction cut-off was found for both SOPC and PSOH dilution demonstrates that differences in mobility of the Cu-IDA group at 3 mN m^{-1} do not strongly impact streptavidin binding or crystallization processes.

5. Interfacial signaling of crystal formation by pyrene-IDA lipids

Fluorescently labeled 'bystander' lipids are frequently employed when studying 2D phase transitions in lipid monolayers or 2D crystallization of proteins by fluorescence microscopy [50]. In our systems, the protein receptor Cu-PSIDA [Fig. 1(A)] is fluorescent by virtue of its pyrene label and has the advantage of optically signaling the presence of protein crystals at the interface directly. Similar to Cu-DOIDA, Cu-PSIDA lipid monolayers were found to target and promote streptavidin crystallization. Cu-PSIDA optically signaled streptavidin crystal formation through quenching of its excimer fluorescence emission. The fluorescence micrographs in Fig. 7 were obtained when streptavidin crystallization was essentially complete. Fig. 7(A) was visualized using the rhodamine label from strep-

tavidin, while Fig. 7(B) was visualized using pyrene excimer fluorescence from Cu-PSIDA. Regions of crystalline streptavidin [bright rhodamine fluorescence, Fig. 7(A)] correspond to regions of quenched Cu-PSIDA excimer fluorescence [Fig. 7(B)]. Areas of the monolayer which contain bound, but non-crystalline, streptavidin do not noticeably quench Cu-PSIDA fluorescence. Fluorescence quenching of the pyrene-labeled Cu-PSIDA lipid by streptavidin crystals shows that photolabeled protein is not required for detecting microstructure formation at the interface. As a complement to BAM, this fluorescence quenching application is potentially useful for proteins which are either difficult to label fluorescently, or where multiple labeling sites interfere with protein–protein interactions and ultimately suppress crystallization.

The effect of protein density on lipid mobility may provide a possible explanation for Cu-PSIDA quenching by streptavidin crystals. When streptavidin binds to the Cu-PSIDA or Cu-DOIDA monolayer, significant increases in surface pressure are observed (from 3 to 12 mN m^{-1} [22]). This indicates the protein is inserting into the monolayer. Lipid mobility may be reduced significantly above the crystals where the protein density is high, hindering the formation of pyrene excimers. Alternatively, reduction in pyrene excimer formation may be due to collisional or static quenching by streptavidin amino acid residues which have penetrated the hydrocarbon region of the monolayer.

6. Conclusions

The streptavidin crystallization experiments with Cu-IDA lipid monolayer systems show that proteins can be specifically targeted to metallated lipid monolayers via coordination of their surface exposed histidine residues. Fluid phase Cu-IDA monolayers can then promote the lateral organization and long-range assembly of bound protein into discrete crystalline structures. We have shown with streptavidin that the coordination of only two surface histidines per protein is sufficient for binding and crystallization. Whether a single surface histidine can mediate these processes remains to be determined. The Cu-IDA lipid monolayers provide a potentially general method for the binding, orientation, and 2D crystallization of proteins at interfaces.

Molecular level packing in streptavidin 2D crystals grown with Cu-IDA lipids is very similar to that in crystals obtained with biotinylated lipids. Micrometer scale crystal morphologies, however, differ significantly between biotin and Cu-IDA lipid monolayer systems. These morphological differences might reflect changes in streptavidin conformation upon binding to biotin, which may not occur with Cu-IDA binding. We have also shown that fluorescently labeled pyrene-Cu-IDA lipids can signal interfacially bound protein crystals.

The potentially general applicability of Cu-IDA monolayers may provide new opportunities in materials science and structural biology. A thorough understanding of protein and monolayer physical properties and their effects on protein binding, nucleation and crystallization may afford new routes to preparing protein-

based materials which require robust (crystalline) arrays. Also, strategically adding or rearranging protein surface histidines to alter protein orientation under Cu-IDA monolayers may facilitate the 2D crystallization of proteins which are otherwise difficult to crystallize. 2D crystals can provide protein structural information directly or serve as templates for the growth of 3D crystals.

Acknowledgements

We gratefully acknowledge support from the Office of Naval Research (FHA), the Army Research Office (FHA), NASA (NAG8-1149 to VV), a National Institute of General Medical Sciences, National Institutes of Health post-doctoral fellowship (1 F32 GM 1632, KMM), and an NIH Training Grant in Biotechnology and Molecular Biophysics (WRS).

Appendix A. Nomenclature

DOIDA	1,1′-[[9-[2,3-bis[(*Z*)-octadec-9-enyloxy]propyl]-3,6,9-trioxanonyl]imino] × diacetic acid
PSIDA	1,1′-[[[2-octadecyloxy,3-(9-pyrenylnonyloxy)propyl]-3,6,9-trioxanonyl] × imino]diacetic acid
PSOH	[2-octadecyloxy,3-(9-pyrenylnonyloxy)propyl]-3,6,9-trioxanonanol
DOPC	L-a-1,2-dioleoyl-sn-3-phosphatidylcholine
SOPC	L-a-1-stearoyl,2-dioleoyl-sn-3-phosphatidylcholine

References

[1] M. Ahlers, W. Müller, A. Reichert, H. Ringsdorf, J. Venzmer, Angew. Chem. Int. Ed. Engl. 29 (1990) 1269.
[2] R.D. Kornberg, S.A. Darst, Curr. Opin. Struct. Biol. 1 (1991) 642.
[3] A.J. Avila-Sakar, W. Chiu, Biophys. J. 70 (1996) 57.
[4] J.H. Fendler, Membrane Mimetic Chemistry: Characterizations and Applications of Micelles, Microemulsions, Monolayers, Bilayers, Vesicles, Host–Guest Systems, and Polyions, Wiley-Interscience, New York, 1982.
[5] S. Mann, D.D. Archibald, J.M. Didymus, T. Douglas, B.R. Heywood, F.C. Meldrum, N.J. Reeves, Science 261 (1993) 1286.
[6] M. Sara, U.B. Sleytr, Progr. Biophys. 65 (1996) 83.
[7] G.L. Gaines, Insoluble Monolayers at Gas–Liquid Interfaces, Interscience, New York, 1966.
[8] S.A. Hemming, A. Bochkarev, S.A. Darst, R.D. Kornberg, P. Ala, D.S.C. Yang, A.M. Edwards, J. Mol. Biol. 246 (1995) 308.
[9] S.A. Darst, M. Ahlers, E.W. Kubalek, P. Meller, R. Blankenburg, H.O. Ribi, H. Ringsdorf, R.D. Kornberg, Biophys. J. 59 (1991) 387.
[10] E.E. Uzgiris, R.D. Kornberg, Nature 301 (1983) 125.
[11] M. Ahlers, R. Blankenburg, P. Meller, H. Ringsdorf, C. Salesse, Thin Solid Films 180 (1989) 93.

[12] L. Lebeau, S. Olland, P. Oudet, C. Mioskowski, Chem. Phys. Lipids 62 (1992) 93.
[13] L. Lebeau, P. Oudet, C. Mioskowski, Helv. Chim. Acta 74 (1991) 1697.
[14] L. Lebeau, E. Regnier, P. Schultz, J.C. Wang, C. Mioskowski, P. Oudet, FEBS 267 (1990) 38.
[15] T. Furuno, H. Sasabe, Biophys. J. 65 (1993) 1714.
[16] S. Ohnishi, M. Hara, T. Furuno, T. Okada, H. Sasabe, Biophys. J. 65 (1993) 573.
[17] A. Sato, T. Furuno, C. Toyoshima, H. Sasabe, Biochim. Biophys. Acta 1162 (1993) 54.
[18] D.R. Shnek, D.W. Pack, D.Y. Sasaki, F.H. Arnold, Langmuir 10 (1994) 2382.
[19] K. Ng, D.W. Pack, D.Y. Sasaki, F.H. Arnold, Langmuir 11 (1995) 4048.
[20] L. Schmitt, C. Dietrich, R. Tampé, J. Am. Chem. Soc. 116 (1994) 8485.
[21] E.W. Kubalek, S.F.J. Legrice, P.O. Brown, J. Struct. Biol. 113 (1994) 117.
[22] D. Pack, G. Chen, K.M. Maloney, C.-T. Chen, F.H. Arnold, J. Am. Chem. Soc. 119 (1997) 2479.
[23] C. Dietrich, L. Schmitt, R. Tampé, Proc. Natl. Acad. Sci. USA 92 (1995) 9014.
[24] A.E. Martell, R.M. Smith, Critical Stability Constants, Plenum Press, New York, 1975.
[25] R.D. Johnson, R.J. Todd, F.H. Arnold, J. Chromatogr. A 725 (1996) 225.
[26] R.J. Todd, R.D. Johnson, F.H. Arnold, J. Chromatogr. A 662 (1994) 13.
[27] F.H. Arnold, B.L. Haymore, Science 252 (1991) 1796.
[28] F.H. Arnold, Bio/Technology 9 (1991) 151.
[29] A.E. Martell, R.M. Smith, Critical Stability Constants, Plenum Press, New York, 1974.
[30] W.A. Hendrickson, A. Pahler, J.L. Smith, Y. Satow, E.A. Merritt, R.P. Phizackerley, Proc. Natl. Acad. Sci. USA 86 (1989) 2190.
[31] A. Pahler, W.A. Hendrickson, M.A. Kolks, C.E. Argarana, C.R. Cantor, J. Biol. Chem. 262 (1987) 13933.
[32] P.C. Weber, D.H. Ohlendorf, J.J. Wendoloski, F.R. Salemme, Science 243 (1989) 85.
[33] P.C. Weber, J.J. Wendoloski, M.W. Pantoliano, F.R. Salemme, J. Am. Chem. Soc. 114 (1992) 3197.
[34] W. Frey, W. Schief, D.W. Pack, C.-T. Tsen, A. Chilkoti, P. Stayton, V. Vogel, F.H. Arnold, Proc. Natl. Acad. Sci. USA 93 (1996) 4937.
[35] V. Vogel, W.R. Schief, W. Frey, Supramol. Sci. 4 (1997) 163.
[36] D.W. Grainger, A. Reichert, H. Ringsdorf, C. Salesse, FEBS Lett. 252 (1989) 79.
[37] D. Hönig, D. Möbius, J. Phys. Chem. 95 (1991) 4590.
[38] S. Hénon, J. Meunier, Rev. Sci. Instrum. 62 (1991) 936.
[39] A.C. Ku, S.A. Darst, C.R. Robertson, A.P. Gast, R.D. Kornberg, J. Phys. Chem. 97 (1993) 3013.
[40] R. Blankenburg, P. Meller, H. Ringsdorf, C. Salesse, Biochemistry 28 (1989) 8214.
[41] W. Frey, W.R. Schief, V. Vogel, Langmuir 12 (1996) 1312.
[42] A. Chilkoti, P.H. Tan, P.S. Stayton, Proc. Natl. Acad. Sci. USA 92 (1995) 1754.
[43] D.W. Pack, F.H. Arnold, Chem. Phys. Lipids 86 (1997) 135.
[44] R.D. Nargessi, D.S. Smith, Methods Enzymol. 122 (1986) 67.
[45] G. Weidemann, U. Gelhert, D. Vollhardt, Langmuir 11 (1995) 864.
[46] I. Langmuir, V.J. Schaefer, D.M. Wrinch, Science 85 (1937) 76.
[47] W. Frey, J. Brink, W.R. Schief, Jr., W. Chiu, V. Vogel, Biophys. J. 74 (1998) 2674.
[48] D. Vaknin, K. Kjaer, J. Als-Nielsen, M. Losche, Biophys. J. 59 (1991) 1325.
[49] A.C. Ku, S.A. Darst, R.D. Kornberg, C.R. Robertson, A.P. Gast, Langmuir 8 (1992) 2357.
[50] R.M. Weiss, Chem. Phys. Lipids 57 (1991) 227.
[51] N.M. Green, Methods Enzymol. 184 (1990) 51.